NMR signal loss from turbulence: Models of time dependence compared with data

Dean O. Kuethe* and Jia-Hong Gao†
Francis Bitter National Magnet Laboratory, Massachusetts Institute of Technology, Cambridge, Massachusetts 02139
(Received 12 October 1994)

This paper reviews theoretical models of nuclear magnetic resonance signal loss due to turbulence in the presence of a magnetic gradient and presents measurements of signal loss from pipe flow as a function of echo time. The models all treat homogeneous turbulence as a random velocity superimposed on a steady velocity. Theoretical signal losses were calculated using previous hot wire anemometry data from dynamically similar air flow. Theoretical pipe cross sections were partitioned into nine concentric homogeneous regions with distinct turbulent diffusivities and intensities. Experimental pipes were 0.95 and 5.0 cm diameter with average water velocities of 1 m s^{-1} providing Reynolds numbers of 12 000 and 55 000. Magnetic gradient strengths ranged from 0.01 to 0.04 G cm^{-1}; echo times ranged from 24 to 120 ms. The models that include the decay of the velocity autocorrelation with time (i.e., consider that turbulence appears more diffusive as the observation time increases) fit the data better than those that do not.

PACS number(s): 47.27.Qb, 76.60.Lz, 47.55.−t, 47.60.+i

I. INTRODUCTION

Nuclear magnetic resonance (NMR) is emerging as a promising tool for measuring statistical properties of turbulence. Measurements depend on an accurate model of NMR signals in the presence of turbulence. Models of this nature are of intrinsic interest to NMR scientists as they are closely related to the broader field of measuring diffusion with NMR.

There have been several models proposed showing how NMR signals decay with time as a function of statistical parameters of turbulence. de Gennes [1] derived expressions for echo amplitudes in a multiple echo train,

$$s=s_0\exp\left[-\frac{23n}{30}\gamma^2G^2\alpha\varepsilon\tau^5\right] \quad \text{for even echoes,} \tag{1}$$

$$s=s_0\exp[-\tfrac{1}{2}\gamma^2G^2\langle u_L^2\rangle\tau^4+\tfrac{7}{30}(n+1)\gamma^2G^2\alpha\varepsilon\tau^5] \quad \text{for odd echoes,} \tag{2}$$

where s_0 is the signal amplitude of stationary liquid, γ is the gyromagnetic ratio, G is the magnitude of a constant magnetic flux density gradient, $\langle u_L^2\rangle$ is the mean of squared Lagrangian velocity fluctuations in the direction of the gradient, τ is $\frac{1}{2}$ the time interval of refocusing radio pulses, n is the echo number, ε is the power dissipation per unit mass, and α is a numerical coefficient. These formulas were derived from the ensemble averages of spin phases with a Gaussian distribution.

DeVille and Landesman [2] experimentally verified different envelopes for the odd and even echo trains. Fukuda and Hirai [3], allowing for the spin phase distribution being Lorentzian and then Gaussian, found that the expressions

$$s=s_0\exp(-\tfrac{1}{2}\gamma^2G^3\langle u_L^2\rangle\tau^4-\gamma Gm\tau^3) \quad \text{for the first echo ,} \tag{3}$$

$$s=s_0\exp(-2\gamma Gm\tau^3) \quad \text{for the second echo ,} \tag{4}$$

where m is a Lorentzian diffusion coefficient, fit their data with respect to the dependence on G better than deGennes's model. The power of 3 exponent of G in (3) was a misprint [4]. Fukuda *et al.* [5] quote the expression for the first echo as

$$s=s_0\exp(-\tfrac{1}{2}\gamma^2G^2\langle u_L^2\rangle\tau^4), \quad \text{when} T_{c_L}>\tau , \tag{5}$$

where T_{c_L} is the Lagrangian correlation time.

Kuethe [6] suggested adding a diffusion term to the modified Bloch equations of Stejskal [7], analogous to the molecular diffusion term but containing turbulent diffusivity (a.k.a. eddy diffusivity) rather than molecular diffusivity. The amplitude of the first echo after signal loss from a constant gradient and scalar turbulent diffusivity D_t is

$$s=s_0\exp(-\tfrac{2}{3}\gamma^2G^2D_t\tau^3) . \tag{6}$$

This is the same expression as that of Carr and Purcell [8] or Stejskel and Tanner [9] with molecular diffusivity replaced by turbulent diffusivity. Kuethe pointed out that D_t, measured with NMR, will not appear constant with echo time unless the echo time is longer than the amount of time it takes the average fluid parcel to change direction a few times, i.e., the apparent turbulent diffusivity will increase from zero and approach an asymptote after a few Lagrangian correlation times.

Gao and Gore [10] derived an expression for echo amplitudes from the ensemble average of spin phases with a Gaussian distribution, assuming an autocorrelation function that decays exponentially,

*Author to whom correspondence should be addressed. Current address: The Lovelace Institutes, 2425 Ridgecrest Drive SE, Albuquerque, NM 87108-5127; electronic address: dkuethe@audrey.tli.org

†Present address: University of Texas Health Sciences Center, 7703 Floyd Curl Drive, San Antonio, TX 78284-6240.

$$s=s_0\exp\left[-n\gamma^2G^2\langle u_L^2\rangle T_{c_L}[\tfrac{2}{3}\tau^3-2\tau T_{c_L}^2+T_{c_L}^3(3-4e^{-\tau/T_{c_L}}+e^{-2\tau/T_{c_L}})]\right.$$
$$\left.+\gamma^2G^2\langle u_L^2\rangle T_{c_L}^4(1-e^{-\tau/T_{c_L}})4\frac{(n-1)(1+e^{-2n\tau/T_{c_L}})+e^{-4\tau/T_{c_L}}+(-1)^n e^{-4n\tau/T_{c_L}}}{(1-e^{-4\tau/T_{c_L}})^2}\right]. \quad (7)$$

If all terms of the Taylor expansion (Appendix) of the exponent in $\tau^n/T_{c_L}^{n-3}$ higher than fifth order are discarded, (7) reduces to

$$s=s_0\exp\left[-\frac{23n}{30}\gamma^2G^2\langle u_L^2\rangle\frac{\tau^5}{T_{c_L}}\right] \quad \text{for even echoes ,} \quad (8)$$

$$s=s_0\exp\left[-\tfrac{1}{2}\gamma^2G^2\langle u_L^2\rangle\tau^4+\left[\frac{37n}{30}-1\right]\gamma^2G^2\langle u_L^2\rangle\frac{\tau^5}{T_{c_L}}\right] \quad \text{for odd echoes ,} \quad (9)$$

which are similar in form to (1) and (2) but do not include energy-dissipation. The expression for the first echo,

$$s=s_0\exp\{-\gamma^2G^2\langle u_L^2\rangle T_{c_L}[\tfrac{2}{3}\tau^3-2\tau T_{c_L}+T_{c_L}^3(3-4e^{-\tau/T_{c_L}}+e^{-2\tau/T_{c_L}})]\}, \quad (10)$$

reduces to (5) for $\tau\ll T_{c_L}$ when all terms except the first of the Taylor expansion are discarded. Gao and Gore consider Eq. (5) to be a simplification of deGennes's Eq. (2). For observation times substantially longer than T_{c_L}, Gao and Gore's interpretation of Taylor's [11] turbulence theory leads to

$$D_t=\langle u_L^2\rangle T_{c_L}, \quad (11)$$

which allows for the reduction of (10) to (6) for $\tau\gg T_{c_L}$ [i.e., $\lim(s)_{T_{c_L}/\tau\to 0}$]. Gao and Gore's data indicate that the signal with increasing gradient strength is proportional to e^{-G^2}.

To derive an expression for the method of Kuethe for cases where T_{c_L} is on the order of or greater than τ, consider a typical expression for the apparent diffusivity that is given by Csanady [12],

$$D_{t_a}=D_t\left[1-\exp\left[\frac{-t}{T_{c_E}}\right]\right], \quad (12)$$

where T_{c_E} is the Eulerian correlation time. For values of $t\ll T_{c_E}$, (12) is approximated to first order by

$$D_{t_a}=\frac{D_t t}{T_{c_E}}. \quad (13)$$

When the apparent diffusivity of (12) is substituted for a diffusion coefficient in modified Bloch equations, the solution under Stejskal's [7] conditions is

$$s=s_0\exp\{-\gamma^2G^2D_t(\tfrac{2}{3}\tau^3+2T_{c_E}^2[T_{c_E}e^{-2\tau/T_{c_E}}+2\tau e^{-\tau/T_{c_E}}-T_{c_E})]\}, \quad (14)$$

for the signal loss from turbulence at the first spin echo. Equation (14) is similar to (10) and has the limiting behavior of (6) for $\tau\gg T_{c_E}$.

When the apparent diffusivity of (13) is substituted, the solution is

$$s=s_0\exp\left[-\tfrac{2}{3}\gamma^2G^2\frac{D_t}{T_{c_E}}\tau^4\right] \quad \text{for } \tau\ll T_{c_E}. \quad (15)$$

Because $\langle u_L^2\rangle\approx\langle u_E^2\rangle$, D_t is the same for Lagrangian and Eulerian descriptions, and (11) is reasonable for both descriptions, we expect $T_{c_E}\approx T_{c_L}$. If the Eulerian and Lagrangian correlation times are equal, (11) can be substituted into (15) to produce

$$s=s_0\exp(-\tfrac{2}{3}\gamma^2G^2\langle u_L^2\rangle\tau^4) \quad \text{for } \tau\ll T_{c_E}, \quad \text{if } T_{c_E}=T_{c_L}, \quad (16)$$

which differs from (5) by a factor of $\frac{4}{3}$ in the exponent. Note that if the time constant in (12) were $\frac{4}{3}T_{c_E}$ rather than T_{c_E}, or if $T_{c_E}=\frac{4}{3}T_{c_L}$, (14) would have the same limiting behaviors as (10). The $\tau\gg T_{c_E}$ limit is unchanged by the $\frac{4}{3}$ factor.

Figure 1 shows a comparison of first echo signal loss predicted by the models. The echo time T_E is 2τ. The curve labeled $\tau\gg T_c$ is Eq. (6). It is the limiting behavior for the model of Gao and Gore (GG), Eq. (10), and the model of Kuethe following Stejskal (KS), Eq. (14), when $\tau\gg T_c$, where T_c represents either the Lagrangian or Eulerian correlation time. The curve labeled $\tau\ll T_c$ is Eq. (5) and is the limiting behavior of the GG model and similar to that of the KS model when $\tau\ll T_c$.

In Fig. 2 the negative exponents of the models divided by $\gamma^2G^2D_tT_c^3$ are plotted against T_E/T_c on log-log axes to display the τ^4 dependence (slope =4) of Eq. (5), the τ^3 dependence (slope =3) of Eq. (6), and how Eqs. (10) and (14) have τ^4 dependence for short T_E and τ^3 dependence for long T_E, (the slope changes from 4 to 3). In Fig. 2(a), the KS and GG models have the same limit, Eq. (6), when $\tau\gg T_c$. When $\tau\ll T_c$, the GG model has the limit

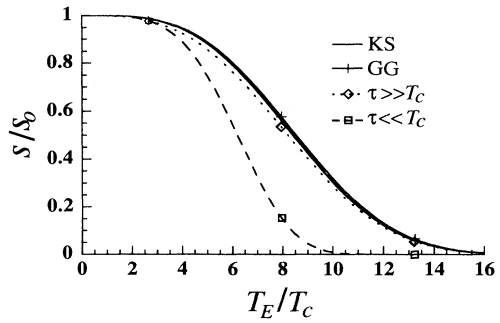

FIG. 1. Predictions of relative amplitude of first echo vs dimensionless echo time for four theories. KS: Kuethe following Stejskal, Eq. (14), assumes apparent turbulent diffusivity increases exponentially with time constant T_c. GG: Gao and Gore, Eq. (10), assumes velocity autocorrelation decreases exponentially with time constant T_c. $\tau \gg T_c$: diffusion theory of Carr and Purcell or Stejskal and Tanner with D_t substituted for molecular diffusivity. $\tau \ll T_c$: first term of deGennes's theory. KS and GG approach $\tau \gg T_c$ for large T_E/T_c and are similar to $\tau \ll T_c$ for small T_E/T_c.

of Eq. (5) and the exponent of KS is $\frac{4}{3}$ larger. In Fig. 2(b) the KS curve is plotted with the $\frac{4}{3}$ factor to show how the KS and GG curves are nearly, but not exactly, congruent when their limits are identical.

While the KS model and the GG model appear very similar in the above comparison, there are important differences between the two. For $\tau < T_c$, the GG model contains the even echo rephasing behavior of deGennes's model and the KS model does not. A second echo KS expression is derived by extending Stejskal's [7] solution to a second echo. Renaming his f as $\mathbf{f}_1$, and introducing $\mathbf{f}_2$, the time integral of the magnetic flux density gradient with π rf pulses at τ and 3τ is expressed as

$$\mathbf{F}-2\zeta\mathbf{f}_1-2\xi\mathbf{f}_2 , \tag{17}$$

where $\mathbf{F}(t)=\int_0^t \mathbf{G}(t')dt'$, $\mathbf{f}_1=\int_0^\tau \mathbf{G}(t')dt'$, $\mathbf{f}_2=\int_\tau^{3\tau}\mathbf{G}(t')dt'$, $\zeta=0$ for $0<t<\tau$, $\zeta=1$ for $\tau<3\tau$, $\zeta=0$ for $3\tau<t<5\tau$, $\xi=0$ for $0<t<3\tau$, and $\xi=1$ for $3\tau<t<5\tau$.

Following Stejskal in seeking the term of the solution that expresses diffusional loss, we seek $B(t)$ that satisfies

$$\frac{d\ln B}{dt}=-\gamma^2(\mathbf{F}-2\zeta\mathbf{f}_1-2\xi\mathbf{f}_2)\cdot\mathbf{D}\cdot(\mathbf{F}-2\zeta\mathbf{f}_1-2\xi\mathbf{f}_2) , \tag{18}$$

which is

$$B(t)=\exp\left[-\gamma^2\left[\int_0^t \mathbf{F}\cdot\mathbf{D}\cdot\mathbf{F}\,dt'-4\zeta\int_0^t \mathbf{F}\cdot\mathbf{D}\cdot\mathbf{f}_1 dt'+4\zeta\int_0^t \mathbf{f}_1\cdot\mathbf{D}\cdot\mathbf{f}_1 dt'-4\xi\int_0^t \mathbf{F}\cdot\mathbf{D}\cdot\mathbf{f}_2 dt'+4\xi\int_0^t \mathbf{f}_2\cdot\mathbf{D}\cdot\mathbf{f}_2 dt'\right]\right] , \tag{19}$$

which is deciphered to

$$B(t)=\exp\left[-\gamma^2\int_0^t\int_0^{t'}\mathbf{G}(t'')dt''\cdot\mathbf{D}\cdot\int_0^{t'}\mathbf{G}(t'')dt''dt'\right], \quad \text{for } 0<t<\tau ,$$

$$B(t)=\exp\left\{-\gamma^2\left[\int_0^t\int_0^{t'}\mathbf{G}(t'')dt''\cdot\mathbf{D}\cdot\int_0^{t'}\mathbf{G}(t'')dt''dt'-4\int_\tau^t\int_\tau^{t'}\mathbf{G}(t'')dt''\cdot\mathbf{D}\cdot\int_0^{\tau}\mathbf{G}(t'')dt''dt'\right]\right\}, \quad \text{for } \tau<t<3\tau ,$$

and

$$B(t)=\exp\left\{-\gamma^2\left[\int_0^t\int_0^{t'}\mathbf{G}(t'')dt''\cdot\mathbf{D}\cdot\int_0^{t'}\mathbf{G}(t'')dt''dt'-4\int_\tau^{3\tau}\int_\tau^{t'}\mathbf{G}(t'')dt''\cdot\mathbf{D}\cdot\int_0^{\tau}\mathbf{G}(\tau'')dt''d\tau'\right.\right.$$
$$\left.\left.-4\int_{3\tau}^t\int_0^{\tau}\mathbf{G}(t'')dt''\cdot\mathbf{D}\cdot\int_\tau^{3\tau}\mathbf{G}(t'')dt''dt'-4\int_{3\tau}^t\int_{3\tau}^{t'}\mathbf{G}(t'')dt''\cdot\mathbf{D}\cdot\int_\tau^{3\tau}\mathbf{G}(t'')dt''dt'\right]\right\},$$
$$\text{for } 3\tau<t<5\tau . \tag{20}$$

For the case of a scalar apparent turbulent diffusivity, Eq. (12), and a constant single component of $\mathbf{G}$, i.e., G, the expression for turbulent signal loss at the second echo 4τ is

$$s=s_0\exp\{-\gamma^2G^2D_t[\tfrac{4}{3}\tau^3+2T_{c_E}^2(T_{c_E}e^{-4\tau/T_{c_E}}+2\tau e^{-3\tau/T_{c_E}}+2\tau e^{-\tau/T_{c_E}}-T_{c_E})]\} , \tag{21}$$

$$s=s_0\exp(-\tfrac{4}{3}\gamma^2G^2D_t\tau^3), \quad \text{for } \tau\gg T_c , \tag{22}$$

$$s=s_0\exp\left[-\tfrac{8}{3}\gamma^2G^2\frac{D_t}{T_{c_E}}\tau^4\right] \quad \text{for } \tau\ll T_c . \tag{23}$$

For comparison, the GG model gives

$$s=s_0\exp\{-\gamma^2G^2\langle u_L^2\rangle T_{c_L}[\tfrac{4}{3}\tau^3-4\tau T_{c_L}^2+T_{c_L}^3(-e^{-4\tau/T_{c_L}}+4e^{-3\tau/T_{c_L}}-4e^{-2\tau/T_{c_L}}-4e^{-\tau/T_{c_L}}+5)]\}\ , \tag{24}$$

$$s=s_0\exp(-\tfrac{4}{3}\gamma^2G_2\langle u_L^2\rangle T_{c_L}\tau^3),\quad \text{for } \tau\gg T_c\ , \tag{25}$$

$$s=s_0\exp\left[-\tfrac{23}{15}\gamma^2G^2\langle u_L^2\rangle\frac{\tau^5}{T_{c_L}}\right]\quad \text{for } \tau\ll T_c\ . \tag{26}$$

The lack of second echo rephasing represented in (23) as opposed to (26) is explained as follows. Equation (12), used to derive Eqs. (21)–(23), implies a truly diffusive process whose diffusion coefficient increases in time rather than a process that appears less coherent with observation time. In a strictly diffusive model, even echo phasing does not occur. In a model with coherent dispersion for $\tau\ll T_c$, even echo rephasing will occur. In order to capture the even echo rephasing behavior in an Eulerian model, one would introduce a stochastic $\mathbf{u}_E$ in the velocity term of the modified Bloch equations instead of introducing $\mathbf{D}_{t_a}$ into a diffusion term. The approach of deGennes extended by Fukuda and Hirai and by Gao and Gore captures the even echo behavior by introducing a stochastic velocity into a Lagrangian description of NMR. Figure 3 shows the divergence of the second echo KS and GG models for short T_{E_2} and their convergence for long T_{E_2}; when both agree the motion is diffusive. It is known from DeVille and Landesman [2] that second echo predictions should include rephasing.

There is a need for experimental evaluation of the signal decay predicted by the models. Their predictions are qualitatively and quantitatively different. The fundamental differences in the relationship of signal amplitude to echo and correlation times can be evaluated by measuring first echo amplitudes. One of the best characterized turbulences is well-developed pipe flow. The distributions of D_t, $\langle u_E^2\rangle$, and T_c can be calculated from published hot-wire anemometry data. The resulting model predictions can be compared to measurements of NMR signal loss.

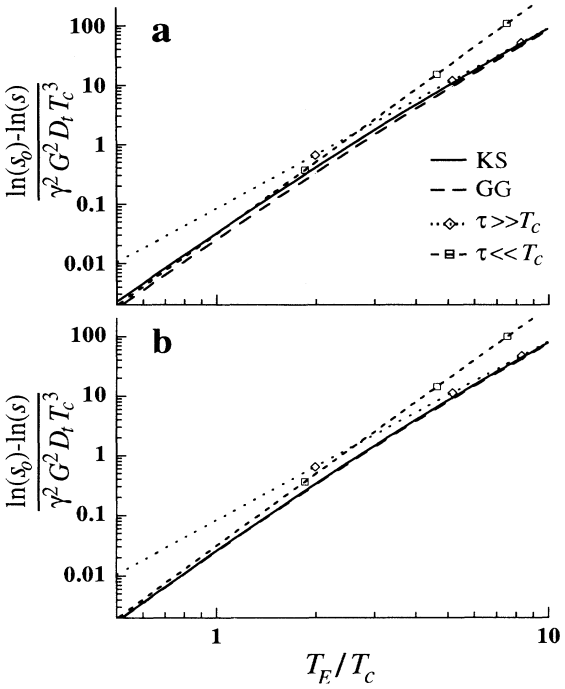

FIG. 2. Scaled negative exponents of theories at first echo vs dimensionless echo time. Exponents of the four theories of Fig. 1 are graphed on log-log axes to display how they vary with echo time. $\ln(s_0)-\ln(s)$ is the negative exponent of the theories. $\gamma^2G^2D_tT_c^3$ is a scaling factor that produces the same curves for different nuclei, magnetic gradient strengths, and turbulence parameters. $\tau\gg T_c$ and $\tau\ll T_c$ are straight lines. KS and GG have the same slope as $\tau\ll T_c$ when T_E/T_c is small and the same slope at $\tau\gg T_c$ when T_E/T_c is large. (a) If $T_{c_E}=T_{c_L}$, KS and GG approach $\tau\gg T_c$ for large T_E/T_c and differ by a factor of $\frac{4}{3}$ as GG approaches $\tau\ll T_c$ for small T_E/T_c. (b) If $T_{c_E}=\frac{4}{3}T_{c_L}$, both limits of KS and GG are the same and the KS and GG curves always predict less signal loss than either $\tau\gg T_c$ or $\tau\ll T_c$. For intermediate values of T_E/T_c, GG predicts slightly less signal loss than KS.

II. MATERIALS AND METHODS

A. Flow apparatus

Two different sizes, 5.0±0.2 cm and 0.95±0.03 cm inside diameter (ID), of acrylic pipe were chosen so that, with an average velocity of approximately 1 m s^{-1}, the larger would provide data for the region in which $\tau\leq T_c$, whereas the smaller would provide data for the region in

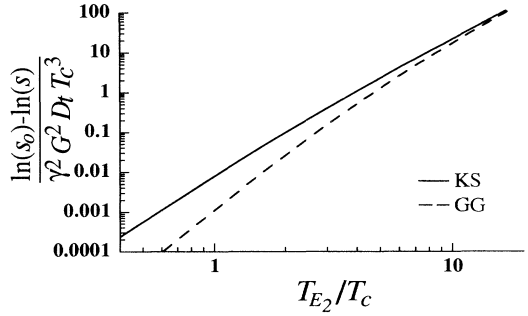

FIG. 3. Scaled negative exponents of KS and GG at second echo vs dimensionless second echo time. For small T_{E_2}/T_c, GG predicts less signal loss due to second echo rephasing. For large T_{E_2}/T_c, GG and KS converge.

which $\tau > T_c$. A constant flow of water was maintained by pumping water up to a reservoir approximately 7 m above the floor and letting it flow through 5.2±0.5-cm polyvinylchloride plumbing and then vinyl flexible hose connected to the test pipes. The outlet was approximately 1 m above the floor. The flow rate was set with a ball valve before the entrance to the flexible hose. An 8-cm ID overflow kept the free surface of the water in the reservoir at a constant height. The flow rate Q was measured by timing the outflow into a graduated cylinder. The water was allowed to flow for an hour before data were collected, because it would gradually heat up until it reached a steady temperature of 28±1 °C (room temperature was 20±1 °C). The average and standard deviations of ten flow rates, five before and five after the experiment, were recorded. The average velocity u_{av} was calculated as Q/A, where A is the cross sectional area of the pipe.

The entrance lengths for the 0.95-cm and 5-cm pipes were 50 and 18 diameters, respectively. The 3 to 4 m of flexible hose leading to the 5-cm pipe was 5.2±0.5 cm ID and had a corrugated surface. The hoses for both pipes were coiled in the bore of the magnet so that the water had at least 4 times the spin-lattice magnetization time constant T_1 to magnetize. The water contained $GdCl_3$ and had a T_1 of 478±50 ms.

In order to compare the models with experimental data, we need values for D_t, $\langle u_L^2 \rangle \approx \langle u_E^2 \rangle$, and $T_{c_E} \approx T_{c_L}$ measured by independent methods. Laufer [13] collected extensive hot-wire anemometry data on velocity fluctuations of turbulent air in well-developed pipe flow. He graphs the distribution of $\sqrt{\langle u_E^2 \rangle}/u_*$ in the radial direction and, from his data, Hinze [14] graphs the distribution of $\nu_t/u_* a$ in the radial direction where ν_t is the eddy viscosity and a is the radius of the pipe. $u_* = \sqrt{[\nu(\partial u/\partial r)]_{\text{at wall}}} = \sqrt{\Delta p a/2L\rho}$ is the friction velocity where $\nu = \mu/\rho$ is the kinematic viscosity of the fluid (μ is viscosity and ρ is density) and Δp is the drop in pressure along length L. We need to rescale the data to the average velocity $u_{av} \equiv Q/A$, making use of the friction factor $\lambda \equiv 8\sigma_w \rho_w / \langle \rho u \rangle^2 = 8u_*^2/u_{av}^2$, where σ_w is the shear stress at the wall. Prandtl's [15] expression for the friction factor in ideally smooth pipes has since been recast [16] as

$$\lambda = (1.82 \log_{10} \mathrm{Re} - 1.64)^{-2} , \tag{27}$$

where Re is the Reynolds number $2u_{av}a/\nu$. From Laufer's pressure and velocity profile data, his friction factor at Re=39 700 was 0.0226, a factor of 1.02 times that predicted by Eq. (27)—a reasonable agreement.

As Re changes, $\nu_t/u_* a$ tends to change less than $\nu_t/u_{av}a$, whereas $\sqrt{\langle u_E^2 \rangle}/u_{av}$ tends to change less than $\sqrt{\langle u_E^2 \rangle}/u_*$. Therefore, the friction factor used for rescaling $\nu_t/u_* a$ to u_{av} was calculated at our experimental pipe's Re, whereas it was calculated at Re=39 700 for rescaling $\sqrt{\langle u_E^2 \rangle}/u_*$.

Eddy viscosity ν_t, the coefficient for diffusion of momentum, is similar to turbulent diffusivity D_t, the coefficient for self-diffusion or mass diffusion of dilute solutes. However, they often differ by up to a factor of 2

TABLE I. Values used to calculate D_t, $\langle u_E^2 \rangle$, and T_c.

Range of $\frac{x}{a}$	$\frac{\nu_t}{u_* a}$	$\frac{\sqrt{\langle u_E^2 \rangle}}{u_*}$
0—0.003125	0.000557	0.0396
0.003125—0.00625	0.00167	0.1147
0.00625—0.0125	0.00334	0.216
0.0125—0.025	0.00668	0.384
0.025—0.05	0.01337	0.617
0.05—0.1	0.0267	0.848
0.1—0.2	0.0454	0.976
0.2—0.5	0.0710	0.938
0.5—1.0	0.0697	0.775

[17]. The calculated value for the average $\nu_t/\nu = (\nu_t/u_* a)_{av}(\mathrm{Re}/2)(u_*/u_{av})$ from Laufer's data at Re=39 700 is 59.3. The average value of D_t/ν calculated from Kuethe's [6] reexamination of Sheriff and O'Kane's [18] diffusion data of nitrous oxide in air pipe flow at Re=60 000 is 110. As a first approximation, D_t is proportional to Re [17], which implies a D_t/ν of 72.8 at Re=39 700—a factor of 1.23 times ν_t/ν. Therefore D_t was taken to be 1.23 times ν_t, with the understanding that the vertical position of the theoretical curves for $\ln(s_0) - \ln(s)$, which is proportional to D_t, is uncertain to within ±25%.

The calculations can be summarized as

$$D_t = 1.23 \frac{\nu_t}{u_* a} \frac{1.02}{\sqrt{8}[1.82 \log_{10}(\mathrm{Re}) - 1.64]} u_{av} a , \tag{28}$$

$$\langle u_E^2 \rangle = \left[\frac{\sqrt{\langle u_E^2 \rangle}}{u_*} \frac{1.02}{\sqrt{8}[1.82 \log_{10}(39\,700) - 1.64]} u_{av} \right]^2 , \tag{29}$$

and

$$T_c = \frac{D_t}{\langle u_E^2 \rangle} . \tag{30}$$

For our calculation, the dimensionless radial position x/a where x is displacement from the wall, was partitioned into nine regions. Values for D_t, $\langle u_E^2 \rangle$, T_c, and theoretical signal losses were calculated for each concentric region, assuming it was homogeneous. Table I lists the values of $\nu_t/u_* a$ and $\sqrt{\langle u_E^2 \rangle}/u_*$ for each region, from Laufer's data.

B. NMR system

The IBM-MIT 1.4 T, 120-cm bore magnet had a field homogeneity of 7 ppm over 50 cm after its superconducting shim currents were optimized. A 35-cm-long 18-cm ID eight-rung, high-pass, birdcage rf coil, built according to Zou [19], was tuned and matched before each use. The linewidths of the water signal from the 0.95 and 5.0-cm pipes were shimmed to within 1 and 2 ppm, respectively. Inhomogeneities caused by the diamagnetism of water

water were at a minimum because the long axis of the pipe was parallel to the static magnetic field. The alteration of the field within such a cylinder should be uniform. Eddy currents from the 80-cm ID Toshiba shielded gradient coils were not detected. The remainder of the system consisted of an Analogic console, rf, and gradient amplifiers.

C. Pulse sequence

The NMR pulse sequence is shown in Fig. 4. The $\pi/2$ rf pulse is nonselective, exciting all the water within the rf coil. The π pulse with accompanying G_z pulse selects 10 cm of water along the z axis, located upstream from the coil's center by $u_{av}T_E/2$, so that when the spin echo forms at T_E, the echo time, the water producing signal will have an average position in the center of the coil. If the pulse sequence were not selective, it would preferentially measure the signal from the water near the walls of the pipe because the faster water excited by the $\pi/2$ pulse could exit the rf coil before the echo is formed. Making the π pulse, rather than the $\pi/2$ pulse, selective reduced the movement of the water between the time of selection and the time of data collection. Appropriate phase cycling and signal averaging were used to eliminate the signal from water that received the $\pi/2$ pulse or the π pulse but not both [$\pi/2$ pulse: $0,0,\pi/2,\pi/2$; π pulse: $0,\pi/2,3\pi/2,0$; averager: $(+I,+Q)$ $(-I,-Q)$, $(-Q,+I)$, $(+Q,-I)$, where I and Q represent the digitized real and imaginary channels of the signal, which are added to or subtracted from the real and imaginary parts of the data]. The rf power was adjusted for each echo time to produce the maximum signal in flowing water in the absence of the G_x pulses.

The magnetic field gradient pulses that produce the desired signal loss are in the x direction, perpendicular to the pipe. There was no signal loss from these pulses due to the average shear because there was no average velocity in the x direction. The first moment of the G_z pulse was only 1.6×10^{-5} G s^{2}m^{-1}, so there was very little signal sacrificed to shear losses for slab selecting. The signal with the G_x pulse was compared to the signal without the G_x pulses to ascertain the signal loss from G_x alone. Because the turbulence in a real pipe is anisotropic, there are cross terms between the G_z pulse and the G_x pulses in complete expressions [e.g, Eq. (20)] of signal loss. They were assumed negligible compared to the loss from G_x. The integrals from Eq. (20) for the weakest, shortest and strongest, and longest G_x pulses were factors of 10 and 16 000 times that for the G_z pulse, respectively, assuming constant D_t. Cross term contributions would be smaller than that from the G_z pulse. The five lobed since rf pulses were 2 ms long and gradient ramps were 1 ms long. The time interval d, $\frac{1}{2}$ the rf pulse duration plus $1\frac{1}{2}$ the gradient ramp duration, was 2.5 ms. The theoretical expressions for signal loss appropriate to the G_x lobes for the pulse sequence are given in the Appendix.

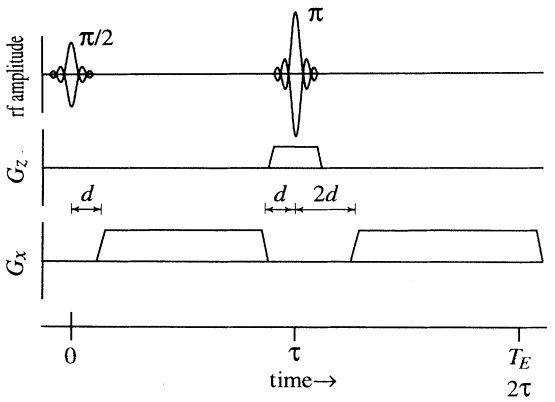

FIG. 4. Pulse sequence. The $\pi/2$ radio pulse is nonselective. The π radio pulse is selective, due to the simultaneous G_z magnetic gradient pulse. A 10-cm slab of water is selected upstream so that the average position of the spins is the center of the rf coil at echo time $T_E=2\tau$. The diffusion sensitizing magnetic gradient pulses G_x cause the desired signal loss. Although G_x is technically a readout gradient, it is not strong enough to broaden the signal linewidth. The time intervals d and τ are used in Eqs. (A1)–(A4) to calculate signal loss.

D. Data collected

The signal was digitized at 64 points, 10 μs apart, and accumulated over the four phase cycles. Signal strength was defined as the sum of the highest three points of the magnitude of the Fourier transformed data. The average of three signal strengths was recorded for each of the echo times 24, 30, 40, 50, 70, 100, and 120 ms with and without the G_x pulses. The signal to noise ratio from water flowing in the absence of G_x pulses was 400 and 1500 for the small and large pipes, respectively, at 100-ms echo time. At 24-ms echo time, the figures were 500 and 2000. The difference in the natural logarithms of the signal strength in the absence and presence of G_x pulses $\ln(s_0)-\ln(s)$ was calculated and compared with that predicted by the theories. The theoretical signal $s_1+s_2+s_3+\cdots+s_9$ was the sum of the signals from each partitioned region.

Three gradient strengths were used for each of the two pipes. Parameters for each of the six experiments are listed in Table II. D_t, $\langle u_E^2\rangle$, and T_c in the table are the average values, weighted by the cross sectional areas of the partitioned regions. To calculate Re, 8.27×10^{-4}kg m^{-1} s^{-1} and 996 kg m^{-3} were used for the viscosity and density, respectively, of the 28±1 °C water.

III. RESULTS

Figure 5 shows a comparison of the theories and data for the six experimental regimes. Dots represent the data. The solid line labeled KS represents Kuethe's [6] use of Stejskal's [7] solutions with an apparent turbulent diffusivity that increases exponentially with time [Eq. (A1)]. The solid line with crosses labeled GG represents Gao and Gore's [10] extension of deGennes's [1] theory with an autocorrelation that decreases exponentially with time [Eq. (A4)]. The dotted line with open diamonds la-

TABLE II. Experimental parameters.

Diameter (cm)[a]	5.0±0.2	5.0±0.2	5.0±0.2	0.95±0.03	0.95±.03	0.95±0.03
u_{av} (cm s^{-1})[a]	89.06±3.66	96.86±3.89	96.86±3.89	106.99±2.20	107.15±1.27	106.99±2.20
Re[a]	53700±6000	58400±6400	58400±6400	12300±1000	12300±700	12300±1000
G (G cm^{-1})[a]	0.01±0.00024	0.015±0.00024	0.02±0.00024	0.02±0.00024	0.03±0.00024	0.04±0.00024
D_t (cm^2 s^{-1})[b]	0.788	0.850	0.850	0.216	0.216	0.216
$\langle u_E^2 \rangle$ (cm^2 s^{-2})[b]	16.7	19.8	19.8	24.1	24.2	24.1
T_c (ms)[b]	48.0	43.7	43.7	9.12	9.10	9.12

[a]Experimentally determined values, errors are $2SD(u_{av}, \mathrm{Re})$, limits of variation (G), or range of diameters measured on different axes (diameter).

[b]Average values for entire cross section, calculated from other sources, applicable to these experiments within ±25%.

beled $\tau \gg T_c$ represents the said limiting behavior of the KS and GG curves [Eq. (A2)]. This is the theory one would obtain using diffusion theories (such as Carr and Purcell [8], and Stejskal and Tanner [9]), with constant turbulent diffusivity substituted for molecular diffusivity. The dashed line with open squares labeled $\tau \ll T_c$ is the said limiting behavior of the KS curve, Eq. (A3), which parallels the limiting behavior of the GG curve, which, in turn, is similar to deGennes's [1] theory and its modification by Fukuda and Hirai [3] as quoted by Fukuda *et al.* [5].

The data appear consistent with the KS and GG curves except the short echo time data from the 5-cm pipe, which appear inconsistent with all the theories and indicate greater signal loss than the KS and GG curves. The open circles in the 5-cm pipe graphs are the values obtained by multiplying the signal in the absence of G_x pulses by 0.966 (see Sec. IV).

Figure 6 shows the dependence of turbulent signal loss on gradient strength. The data are normalized by dividing them by the KS theory values and multiplying them by G^2 so that points from different turbulences and echo times can be displayed on the same graph. The dashed line is valued G^2. It is a quadratic curve representing the assumption that the signal from turbulence varies as e^{-G^2}.

IV. DISCUSSION

There appears to be more signal loss at short echo times in the larger pipe than is consistent with the small

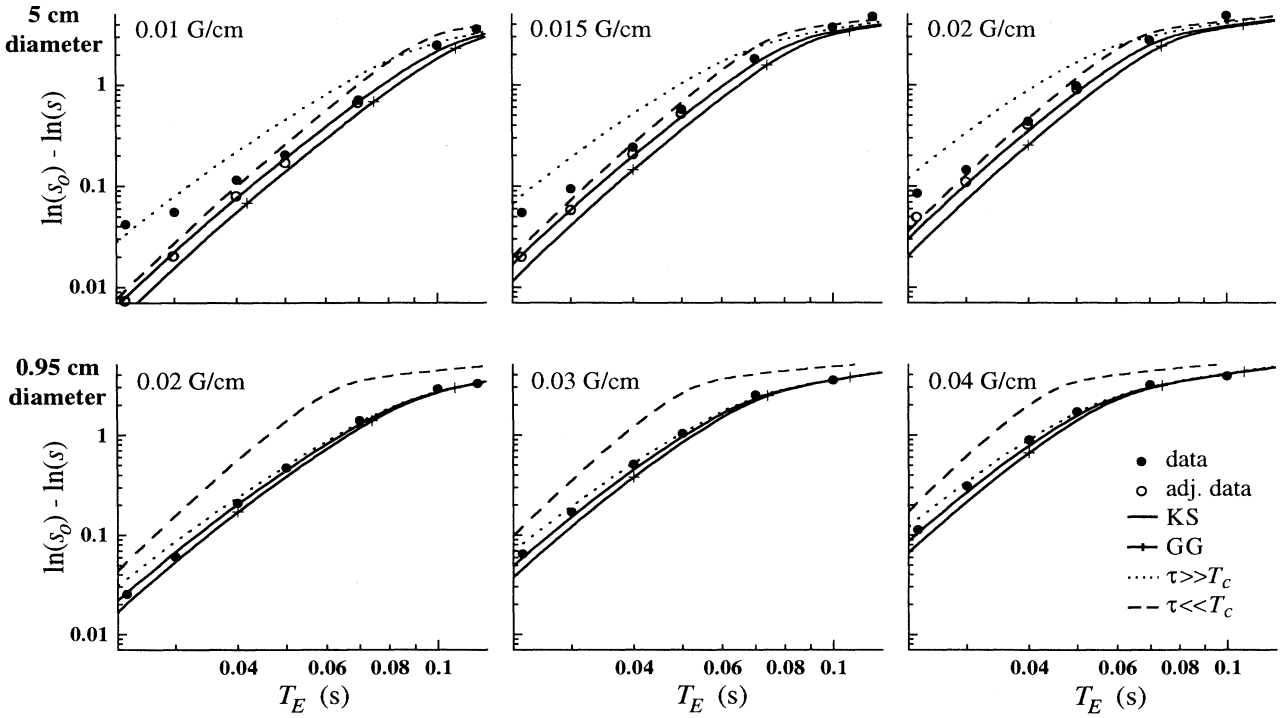

FIG. 5. Data compared with theories. $\ln(s_0) - \ln(s)$ is shown for data, adjusted data, and theories vs. echo time. For data, s is the signal strength in the presence of G_x pulses and s_0 is the signal strength in their absence. The adjusted data for the 5-cm diameter pipe (top graphs) have s_0 multiplied by 0.966. For theories, s is the sum of signals from the nine regions of the partitioned pipe cross section with $s_0 = 1$. The strength of G_x for the six data sets label each graph. KS, $\tau \gg T_c$, $\tau \ll T_c$, and GG are calculated using Eqs. (A1)–(A4), respectively. $\tau \ll T_c$ is the said limit of KS, which is $\frac{4}{3}$ that of GG.

pipe data or the theories. This is probably due to the signal in the absence of the G_x pulse being too high rather than the signal in their presence being too low. Incomplete cancellation of the free induction decay (FID) from spins excited by the nonselective $\pi/2$ rf pulse that are not refocused by the selective π pulse would add a baseline signal to the spin echo, making it too high. In principle, the FID is canceled by rf phase cycling, but the flowing spins move through an inhomogeneous field, distorting their phases to foil perfect cancellation. When the G_x pulse is turned on, the FID is canceled so the baseline signal is removed, creating an apparent signal loss. The effect of a baseline signal is especially strong when the true signal loss is low. Multiplying the signal in the absence of G_x by 0.966 brings the short echo time points into congruence with the KS and GG curves (open circles in Fig. 5) without significantly displacing the other points on the graph.

Facts supporting this explanation are as follows: (i) The effect is not apparent in the small pipe, which experiences much less of the magnet's x and y inhomogeneity. (ii) The spectral peak is narrower with the G_x gradient *on* indicating that signal from the greater region of water not receiving the π pulse is being dephased by the applied gradient and not contributing its inhomogeneously broadened signal.

The data support the KS and GG theories satisfactorily in that most of them demonstrate a good fit, and the explanation for departures at short echo times in the 5-cm pipe is compelling. While the data may appear to favor the KS curves over the GG curves, uncertainty in the placement of the theoretical curves prevents a positive assignment. Figure 7 shows the best fit of the data from the larger pipe, for which the theories are more

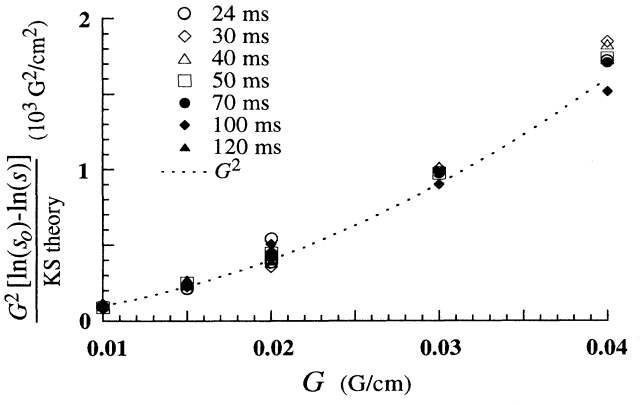

FIG. 6. Signal loss dependence on G. Multiplying $\ln(s_0)-\ln(s)$ by G^2 and dividing by the prediction of the KS theory for $\ln(s_0)-\ln(s)$ provides an axis for graphing all the data from different echo times and turbulences vs G. The adjusted data were used for the 5-cm pipe. The dotted line labeled G^2 represents the assumption that signal loss is modeled by application of the KS theory to the nine partitioned regions of the pipe. If the data points also show quadratic dependence, even though they fall above or below the dotted line, they imply that the signal varies with e^{-G^2}, in accordance with the four theories.

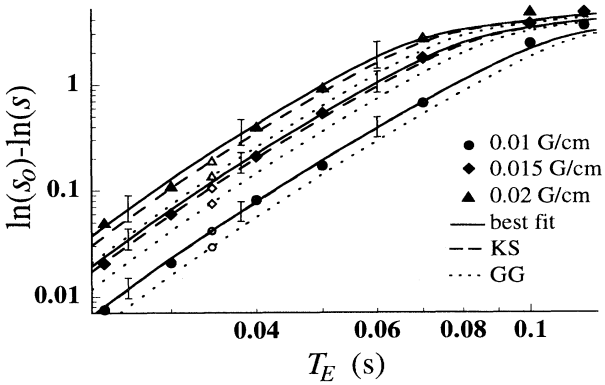

FIG. 7. Statistical comparison of KS and GG theories. The three solid lines are the best fits to the three sets of adjusted 5-cm pipe data with the multiplicative factor of T_{c_E} as a free parameter in the KS theory. The KS theory (dashed lines) implies a factor of 1; the GG theory (dotted lines) is very closely approximated by a factor of $\frac{4}{3}$. Factors are 0.989, 0.866, and 0.774 for the 0.01, 0.015, and 0.02 G cm^{-1} data, respectively. Circles, diamonds, and triangles are used to separate the three data sets. Filled figures represent the data, and open figures mark the KS and GG curves. The solid curves were fit by positioning them so that the mean of the quotients of the data values and curve values is 1. This minimizes the sum of the vertical displacements on the graph. Error bars represent two standard deviations of the quotients about the curves.

divergent. The solid lines were fit to the data by allowing the multiplicative factor of T_{c_E} to be a free parameter in the KS theory and minimizing the linear vertical distance error on the log-log plot (i.e., the mean of the quotients of the data points and the curve values is 1). Minimizing the distance error weights each datum equally and does not favor outliers. The multiplicative factors of T_{c_E} are 0.989, 0.866, and 0.774 for the 0.01, 0.015 , and 0.02 G cm^{-1} data, respectively. The signal in the absence of G_x has been multiplied by 0.966, as mentioned above. The dashed lines represent the KS theory. The dotted lines represent the GG theory. The error bars, derived from the curve fit, represent two standard deviations in the quotients. They include the KS curves but not the GG curves.

The uncertainty in calculating D_t and $\langle u_E^2 \rangle$ in our pipes from Laufer's [13] data means that the theoretical curve placements are only accurate to 25%. The 25% placement uncertainty and the average curve fitting error of 24% indicate that factors, within 49% cannot be distinguished with certainty. The KS and GG curves differ in the 24–70 ms range by only 40%, assuming $T_{c_E} = T_{c_L}$.

The KS and GG theories are favored over either of the theories that assume very long or very short T_c. This implies that in order to measure either turbulent intensity or diffusivity with NMR signal attenuation in a magnetic field gradient, it is necessary to have a measurement of the correlation time. In order to use the $\tau \gg T_c$ or $\tau \ll T_c$ approximations, one must know that the echo time and the correlation time differ by a factor of 10 or more.

NMR measurements of turbulence have small dynamic range because of low signal to noise ratios and because small signal losses will give an unreliable measurement. For example, assume that the signal to noise ratio in the absence of dephasing pulses is 1000:1, $s_0=1000$, and a measurement of D_t is sought. The difference between $s=999$ and $s=998$ implies a factor of 2 in D_t. Recall how a small adjustment in s_0 made a large difference in the low signal loss data in Fig. 5. Changes of 1 near $s=980$ cause a more reasonable 5% change. Changes of 1 also imply large factors in D_t for signals below 4. The useful range of s, 4 to 980, leads to a factor of 550 for D_t.

Kuethe [6] noted that his measured diffusivities appeared to be low by a factor of 2. He made measurements at different echo times and considered the turbulent diffusivity in a 0.95-cm ID pipe to be the asymptotic value that the apparent diffusivity (measured assuming $\tau \gg T_c$) approached at longer echo times. The factor of 1.067 between the full KS expression vs the $\tau \gg T_c$ approximation, and the factor of 1.043 that would arise from signal recovery from the moment nulled gradients were small compared to the factor of 2. However, his assumption that one average value of D_t adequately described the signal loss overestimated the expected signal at long echo times. Figure 8 shows how, in the present 0.95-cm pipe, the theoretical signal loss diverges from the data at long echo times if the average values of D_t, $\langle u_E^2 \rangle$, and T_c over the cross section are used to calculate the signal loss. The departure can easily account for a factor of 2 and indicates that pipe turbulence cannot be treated as homogeneous in NMR experiments.

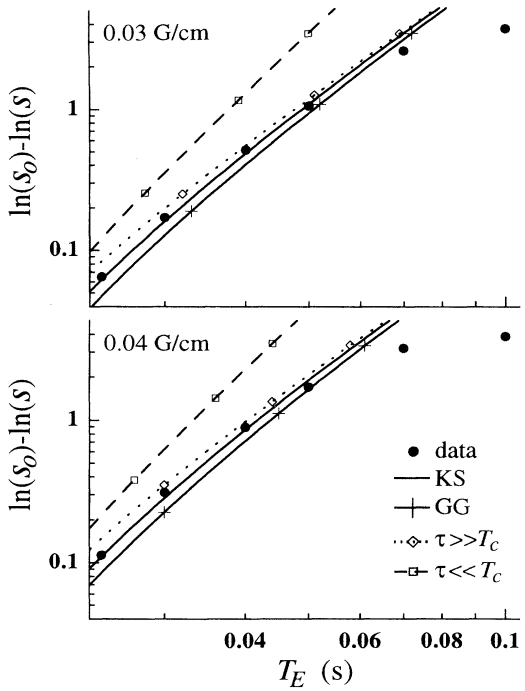

FIG. 8. Disparity of 0.95-cm pipe data and theory if pipe turbulence is assumed to be homogeneous. The theoretical curves are graphed with the average values of D_t, $\langle u_E^2 \rangle$, T_c rather than summing the signal from nine different regions with different values of D_t, $\langle u_E^2 \rangle$, T_c. At shorter T_Es, when the signal is coming from the bulk of the water, the predictions are reasonable. At longer T_Es, when the remaining signal is coming primarily from near the walls, the data and theoretical curves are disparate. The average values of D_t, $\langle u_E^2 \rangle$, T_c are not representative of the turbulence near the walls.

We emphasize two important differences between the KS and GG models. One is that the KS model does not exhibit even echo rephasing when $\tau < T_c$ whereas the GG model does. This difference will also be apparent in pulse sequences in which the first moment of the magnetic gradient is zero near data collection because in both models, π rf pulses have the same effect as changing the sign of all subsequent gradient pulses.

The second difference is that the KS model is a Eulerian description of the moment densities at all points, whereas the GG model is an ensemble average of all spins from a Lagrangian viewpoint. There is a measurable difference between the two theories that is a result of this difference in viewpoints. The KS model predicts that if $\int_0^{t_l} \mathbf{G}(t)dt \neq 0$, after magnetic gradient pulses are turned off at time t_l, the signal will decrease with e^{-t}; the GG model predicts that signal loss stops after gradient pulses end. According to the KS model, increasingly different spins from an increasingly greater area get mixed at any given point as time progresses. According to the GG model, the absence of a gradient implies no further dispersion in phases. The predicted difference is not ablated by integrating the KS model over a limited region of space because differing spins from the surrounding will continue to diffuse into the region. [Integrating over infinite space when $\int_0^{t_l} \mathbf{G}(t)dt \neq 0$ results in no signal.] The difference, which applies to molecular as well as turbulent diffusion, has not been tested experimentally, to our knowledge.

A Eulerian description has an intrinsic appeal for imaging because it provides the distribution of magnetic moment density at echo time. In Lagrangian descriptions, spin phases are known but their whereabouts are uncertain. Another advantage to the KS model is that the signal loss from all the magnetic gradient pulses in a complicated sequence can be calculated from elementary integrals that include provisions for anisotropic diffusion coefficients.

It is important to remember that none of the expressions in this paper are correct as written for turbulence characteristics that vary in space. The error in using the Eulerian expressions derived from overly simplified initial and boundary conditions can be estimated, as in Ref. [6], or calculated by comparing the expressions with numerical solutions from more appropriate conditions. In the present experiment, theories of homogeneous turbulence were applied to nine different regions of pipe turbulence, each assumed to be homogeneous. The success of the method indicates that, under the current experimental conditions, the error in total signal amplitude from applying the expressions to inhomogeneous turbulence (reducing the mesh of the partition to zero) is small. Nonetheless, estimates for errors in applying such expressions to imaging "voxels" are significant if turbulence is

inhomogeneous [6].

Kuethe concluded [6] that magnetohydrodynamic damping is insignificant in weak salt solutions at 1.5 T, because of low values of the Hartman and Lundquist numbers [6]. The agreement of the present data with what is predicted from previous knowledge of air flow in the earth's magnetic field supports this conclusion.

In summary, the first echo amplitude predictions of the KS and GG models are supported by the data. In order to measure either turbulent intensity of diffusivity with NMR signal attenuation in a magnetic field gradient, it is necessary to have a measurement of the correlation time. In order to use $\tau \gg T_c$ or $\tau \ll T_c$ approximations, one must know that the echo time and correlation time differ by a factor of 10 or more. Turbulence measurements from NMR signal attenuation have small dynamic range due to low signal to noise ratios. Errors inherent in applying formulas from this paper to inhomogeneous turbulence are significant, but can be estimated.

ACKNOWLEDGMENTS

Many thanks to James Wrenn for technical support with the magnet, console, and rf coil; William Punchard for gradient coil design; Gary Zientara for console software; Analogic Equipment Corp. for the loan of amplifiers; Ain Sonin for fluid mechanics consultation; and Eiichi Fukushima, Allen Waggoner, Lee Wang, Irving Lowe, and Masami Nakagawa for comments on the manuscript. This research was supported by the Toshiba Corporation and the Seiver Foundation.

APPENDIX

Expressions for signal loss from homogeneous turbulence using the pulse sequence shown in Fig. 4 are as follows. For the Keuthe-Stejskal model,

$$s = s_0 \exp\Big(-\gamma^2 G^2 D_t \Big\{ \tfrac{2}{3}\tau^3 - \tau^2 d - 4\tau d^2 + \tfrac{20}{3} d^3 + 2T_{c_E}^2 \Big[T_{c_E} e^{-2\tau/T_{c_E}} + (\tau - T_{c_E} - 2d) e^{-(\tau+2d)/T_{c_E}} + (\tau + T_{c_E} - 2d) e^{-(\tau-d)/T_{c_E}} - T_{c_E} e^{-d/T_{c_E}} \Big] \Big\} \Big) , \tag{A1}$$

which approaches

$$s = s_0 \exp\left[-\gamma^2 G^2 D_t \left(\tfrac{2}{3}\tau^3 - \tau^2 d - 4\tau d^2 + \tfrac{20}{3} d^3 \right) \right] \quad \text{when } \tau \gg T_c , \tag{A2}$$

$$s = s_0 \exp\left[-\gamma^2 G^2 \frac{D_t}{T_{c_E}} \left(\tfrac{2}{3}\tau^4 - \tfrac{2}{3}\tau^3 d - \tfrac{9}{2}\tau^2 d^2 + \tfrac{14}{3}\tau d^3 + \tfrac{10}{3} d^4 \right) \right] \quad \text{when } \tau \ll T_c . \tag{A3}$$

For the Gao and Gore model,

$$s = s_0 \exp\Big(-\gamma^2 G^2 \langle u_L^2 \rangle T_{c_L} \Big\{ \tfrac{2}{3}\tau^3 - \tau^2 d - 4\tau d^2 + \tfrac{20}{3} d^3 - 2(\tau - 2d) T_{c_L}^2 + T_{c_L}^3 \Big[2 - 2e^{-(\tau-2d)/T_{c_L}} - 2e^{-(\tau+d)/T_{c_L}} + e^{-(2\tau-d)/T_{c_L}} + e^{-3d/T_{c_L}} \Big] \Big\} \Big) , \tag{A4}$$

which also approaches (A2) and approaches $\frac{3}{4}$ of (A3) if $T_{c_E} = T_{c_L}$.

Expressions of signal loss from homogeneous turbulence and constant gradient are given below with the exponents expressed in Taylor expansions.

GG first echo,

$$s = s_0 \exp\left\{ -\gamma^2 G^2 \langle u_L^2 \rangle T_{c_L} \left[\tfrac{2}{3}\tau^3 - 2\tau T_{c_L}^2 + \sum_{n=1}^{\infty} \frac{(-1)^n (2^n - 4)\tau^n}{n! T_{c_L}^{n-3}} \right] \right\}$$

$$= s_0 \exp\left[-\gamma^2 G^2 \langle u_L^2 \rangle T_{c_L} \left[\frac{1}{2}\frac{\tau^4}{T_{c_L}} - \frac{7}{30}\frac{\tau^5}{T_{c_L}^2} + \frac{1}{12}\frac{\tau^6}{T_{c_L}^3} - \frac{31}{1260}\frac{\tau^7}{T_{c_L}^4} + \cdots \right] \right] . \tag{A5}$$

GG second echo,

$$s = s_0 \exp\left\{ -\gamma^2 G^2 \langle u_L^2 \rangle T_{c_L} \left[\frac{4}{3}\tau^3 - 4\tau T_{c_L}^2 + 4 \sum_{n=1}^{\infty} \frac{(-1)^n (-4^{n-1} + 3^n - 2^n - 1)\tau^n}{n! T_{c_L}^{n-3}} \right] \right\}$$

$$= s_0 \exp\left[-\gamma^2 G^2 \langle u_L^2 \rangle T_{c_L} \left[\frac{23\tau^5}{15 T_{c_L}^2} - 2\frac{\tau^6}{T_{c_L}^3} + \frac{1019\tau^7}{630 T_{c_L}^4} + \cdots \right] \right] . \tag{A6}$$

KS first echo,

$$s = s_0 \exp\left\{-\gamma^2 G^2 D_t \left[\frac{2}{3}\tau^3 + 2\sum_{n=1}^{\infty} \frac{(-1)^n (2^n - 2n)\tau^n}{n! T_{c_E}^{n-3}}\right]\right\}$$
$$= s_0 \exp\left[-\gamma^2 G^2 D_t \left[\frac{2\tau^4}{3T_{c_E}} - \frac{11\tau^5}{30T_{c_E}^2} + \frac{13\tau^6}{90T_{c_E}^3} - \frac{19\tau^7}{420T_{c_E}^4} + \cdots\right]\right]. \quad \text{(A7)}$$

KS second echo,

$$s = s_0 \exp\left[-\gamma^2 G^2 D_t \left\{\frac{4}{3}\tau^3 + 2\sum_{n=1}^{\infty} \frac{(-1)^n [4^n - 2n(3^{n-1}+1)]\tau^n}{n! T_{c_E}^{n-3}}\right\}\right]$$
$$= s_0 \exp\left[-\gamma^2 G^2 D_t \left[\frac{8\tau^4}{3T_{c_E}} - \frac{17\tau^5}{15T_{c_E}^2} + \frac{146\tau^6}{45T_{c_E}^3} - \frac{1541\tau^7}{630T_{c_E}^4} + \cdots\right]\right]. \quad \text{(A8)}$$

[1] P. G. deGennes, Phys. Lett. **29A**, 20 (1969).
[2] G. DeVille and A. Landesman, J. Phys. (Paris) **32**, 67 (1971).
[3] K. Fukuda and A. Hirai, J. Phys. Soc. Jpn. **47**, 1999 (1979).
[4] K. Fukuda (private communication).
[5] K. Fukuda, A. Inouye, Y. Kawabe, and A. Hirai, J. Phys. Soc. Jpn. **54**, 4555 (1985).
[6] D. O. Kuethe, Phys. Rev. A **40**, 4542 (1989).
[7] E. O. Stejskal, J. Chem. Phys. **43**, 3597 (1965).
[8] H. Y. Carr and E. M. Purcell, Phys. Rev. **94**, 630 (1954).
[9] E. O. Stejskal and J. E. Tanner, J. Chem. Phys. **42**, 288 (1965).
[10] J. -H. Gao and J. C. Gore, Med. Phys. **18**, 1045 (1991).
[11] G. I. Taylor, Proc. London Math. Soc. Ser. 2. **20**, 196 (1921).
[12] G. T. Csanady, *Turbulent Diffusion in the Environment* (Reidel, Boston, 1972), p. 63.
[13] J. Laufer, National Advisory Committee for Aeronautics Report No. 1174, 1954 (unpublished).
[14] J. O. Hinze, *Turbulence* (McGraw-Hill, New York 1975), pp. 730 and 731.
[15] L. Prandtl, Z. V. Deut. Ing. **77**, 105 (1933), cited in H. Schlichting, *Boundary Layer Theory* (McGraw-Hill, New York, 1979), p. 609.
[16] B. S. Petukhov, in *Advances in Heat Transfer,* edited by J. P. Hartnett and T. F. Irving (Academic, New York, 1970), p. 523.
[17] A. Quarmby and R. K. Anand, J. Fluid Mech. **38**, 433 (1969).
[18] N. Sheriff and D. J. O'Kane, Int. J. Heat Mass Transfer **14**, 679 (1971).
[19] X. Zou, Ph.D. thesis, Massachusetts Institute of Technology, 1992.